Adiabatic Passage through Chaos

Amit Dey,[1] Doron Cohen,[2] and Amichay Vardi[1]
[1]Department of Chemistry, Ben-Gurion University of the Negev, Beer-Sheva 84105, Israel
[2]Department of Physics, Ben-Gurion University of the Negev, Beer-Sheva 84105, Israel

(Received 14 May 2018; published 21 December 2018)

We study the process of nonlinear stimulated Raman adiabatic passage within a classical mean-field framework. Depending on the sign of interaction, the breakdown of adiabaticity in the interacting nonintegrable system is not related to bifurcations in the energy landscape, but rather to the emergence of quasistochastic motion that drains the followed quasistationary state. Consequently, faster sweep rate, rather than quasistatic variation of parameters, is better for adiabaticity.

DOI: 10.1103/PhysRevLett.121.250405

The analysis of quasistatic adiabatic processes is a central theme in quantum thermodynamics, coherent control, quantum state engineering, nonlinear and quantum optics, and nanotechnology. The adiabatic paradigm extends from microscopic systems with few degrees of freedom, through mesoscopic nanomachinary to macroscopic steam engines. Throughout this vast range of applications, common wisdom has it that "slow is better," i.e., that excitations from the followed adiabatic state can be avoided by slower variation of the system's control parameters. Here, we show that when chaotic stages are encountered during an adiabatic scenario, slow variation can in fact *damage* its efficiency.

The effect is demonstrated using a minimal example: a stimulated Raman adiabatic passage (STIRAP) [1,2] in the presence of interactions. Advances in Bose-Einstein condensation, nonlinear optics, and the control of light in coupled waveguides [3,4], have triggered great interest in the application of adiabatic passage to interacting systems. The effects of interactions on two-mode adiabatic schemes were studied using various Bose-Hubbard dimer Hamiltonians [5–26]. The common denominator for all these studies is the quest for energetic stability. The dynamics follows a stationary point (SP) of the instantaneous Hamiltonian $H(x)$, where $x = x(t)$ is a control parameter. This SP, that has some x-dependent energy $E(\mathrm{SP})$, is required to be a local minimum (or a local maximum) of the energy landscape. Nonlinear instability is attributed to the emergence of a separatrix in the energy landscape due to a bifurcation of such a SP.

The same energetic stability paradigm was adopted for adiabatic passage in the three-mode trimer [27–31]: The SPs of the energy landscape were found as a function of time, resulting in a bifurcation diagram that reflects topological changes in the energy landscape. Such bifurcations, notably the "horn" avoided crossing in the nonlinear STIRAP case [27], were assumed to cause the breakdown of adiabaticity. However the three-mode system requires a more careful treatment. While the SPs of systems with more than one degree of freedom are typically saddle points of the energy landscape, their *dynamical* stability analysis (e.g., via the Bogoliubov formalism [32,33]) can indicate either stability (real Bogoliubov frequencies) or instability (complex Bogoliubov frequencies). In fact, the full understanding of stability requires a Kolmogorov-Arnold-Moser perspective [34]. The bifurcation diagram lacks this essential information. For the system under study, Poincaré sections are valuable tools for inspecting the mixed chaotic phase-space structure.

Outline.—We show that the adiabatic passage efficiency is drastically affected by the appearance of chaotic regions, whose existence is not related to the SP bifurcation diagram. Consequently, the analysis of adiabatic passage goes beyond the prevailing energetic stability paradigm. Specifically, reduced efficiency in STIRAP is observed even in the absence of avoided crossings. We establish that the breakdown of adiabaticity occurs during specific time intervals in which the followed SP becomes immersed in chaotic strips on the same energy surface. One outcome of this novel breakdown mechanism, is that adiabaticity may be restored by faster variation of the control parameter, so as to guarantee that the dangerous x interval is traversed before the evolving state has the time to spread along the chaotic strip.

STIRAP.—Many-body STIRAP is modeled by the time-dependent Bose-Hubbard trimer Hamiltonian [27,35–42] for N particles in three second-quantized modes,

$$\mathcal{H} = \mathcal{E}\hat{n}_2 + \frac{U}{2}\sum_{j=1}^{3}\hat{n}_i^2 - \frac{1}{2}(\Omega_p(x)\hat{a}_2^\dagger\hat{a}_1 + \Omega_s(x)\hat{a}_3^\dagger\hat{a}_2 + \mathrm{H.c.}). \quad (1)$$

Here, $\hat{a}_j$, $\hat{a}_j^\dagger$ are bosonic operators with associated occupations $\hat{n}_j \equiv \hat{a}_j^\dagger\hat{a}_j$. The interaction strength is U, while $\mathcal{E}$ is

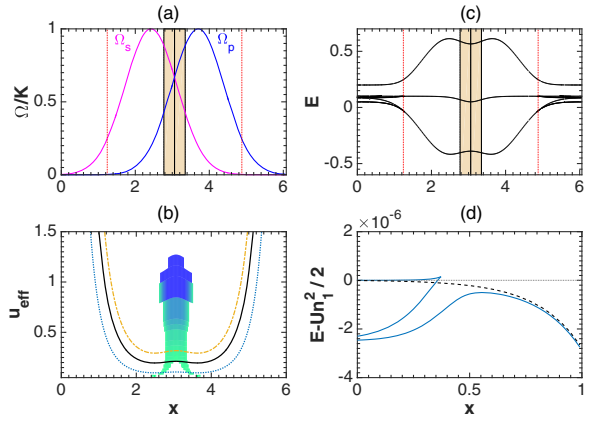

FIG. 1. (a) STIRAP pulse scheme. Throughout the Letter, shaded intervals mark the range where chaos leads to breakdown of adiabaticity, while vertical dotted lines mark the location of the horn avoided crossings. (a),(c) The interaction parameter is $u = 0.2$. Here and in all subsequent figures we set $\varepsilon = 0.1$ for the detuning. (b) The effective interaction parameter $u_{\rm eff}(x)$ for $u = 0.1$ (dotted), 0.2 (solid), 0.3 (dash dotted). The background color indicates the instability of the SP for each (x, u) point: it is white if the Bogoliubov frequencies are real and colored by green to blue to indicate nonzero magnitude of $\mathrm{Im}(\omega)$ (see text). (c) Adiabatic $E(\mathrm{SP})$ energies. The followed state corresponds to the middle curve. (d) Emergence of the horn crossing. The $E(\mathrm{SP})$ of the followed state is enlarged for $u = 0$ (dotted gray), $u = 0.1$ (dashed black), and $u = 0.101$ (solid blue).

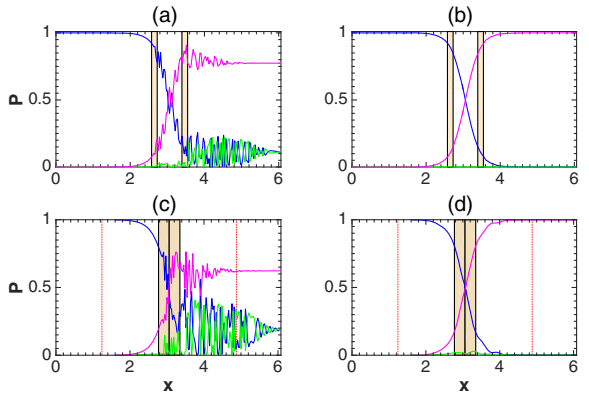

FIG. 2. Evolution of the site populations versus $x(t)$. Locations of the horn crossings (if they exist) and of the chaotic intervals are marked. (a) Failure of STIRAP in the absence of SP bifurcations: here $u = 0.8\varepsilon$ is *below* the critical value for obtaining the horn crossing. The sweep rate is $\dot{x}/K = 6 \times 10^{-5}$. (b) Recovery of adiabatic passage with increased sweep rate ($\dot{x}/K = 6 \times 10^{-4}$) during chaotic intervals. (c) Failure of STIRAP for $u = 2\varepsilon$, with initial conditions that bypass the horn crossing: the process is launched at the adiabatic state after the avoided crossing. Sweep rate is $\dot{x}/K = 6 \times 10^{-4}$. (d) For same u, efficiency is recovered due to faster sweep ($\dot{x}/K = 4 \times 10^{-2}$).

equivalent to the one-photon detuning of the optical scheme [1,2]. In STIRAP, the couplings are Gaussian Stokes and pump pulses $\Omega_{s,p}(x) = Ke^{-(x-x_{s,p})^2}$, which depend on the dimensionless parameter x. The standard realization is a simple constant-rate sweep $x(t) = t/\tau$, with a "counterintuitive" sequence $x_p - x_s > 0$, as shown in Fig. 1(a). The system is prepared in the first mode $[n_1(0) = N]$. For $U = 0$, an adiabatic sweep transfers the population to the third mode $[n_3(\infty) = N]$ by following a coherent dark eigenstate that does not project on the intermediate mode at any time $[n_2(t) = 0]$. The studied effect is the breakdown of this adiabatic 100% efficiency in the presence of repulsive interactions ($U > 0$).

Classical dynamics.—In classical mean-field theory, field operators $\hat{a}_j$ are replaced by c numbers $a_j \equiv \sqrt{n_j}e^{i\phi_j}$. Rescaling $a_j \mapsto a_j/\sqrt{N}$ and $t \mapsto Kt$, and defining $P_j = |a_j|^2$, we obtain the nonlinear Schrödinger equations [27] $i\dot{\mathbf{a}} = (\mathcal{H}_0 + u\mathcal{P})\mathbf{a}$, where

$$\mathcal{H}_0 = \begin{pmatrix} 0 & -\kappa_p/2 & 0 \\ -\kappa_p/2 & \varepsilon & -\kappa_s/2 \\ 0 & -\kappa_s/2 & 0 \end{pmatrix}, \quad \mathcal{P} = \begin{pmatrix} P_1 & 0 & 0 \\ 0 & P_2 & 0 \\ 0 & 0 & P_3 \end{pmatrix}. \tag{2}$$

The dimensionless parameters are the interaction $u = NU/K$, the detuning $\varepsilon = \mathcal{E}/K$, and the couplings $\kappa_{p,s} = \Omega_{p,s}/K$. We also define the effective nonlinearity $u_{\rm eff}(x) = u/[\kappa_p^2(x) + \kappa_s^2(x)]^{1/2}$. The latter is largest at the beginning and at the end of the sweep, where the linear coupling terms are small [see Fig. 1(b)].

Bifurcation diagram.—The steady states of our system (at fixed x) are the SPs of the grand canonical Hamiltonian $\mathcal{H} - \mu N$, satisfying $i\dot{\mathbf{a}} = \mu\mathbf{a}$, where μ is identified as the chemical potential. The solution of this equation has been presented in [27]. The adiabatic energies $E(\mathrm{SP})$ are the value of $\mathcal{H}$ at the SPs. For $u = 0$ there are three SPs, corresponding to the adiabatic eigenstates of linear STIRAP [2]. In the presence of interaction, the SPs bifurcate if the effective interaction $u_{\rm eff}(x)$ is large enough, i.e., at early and late times, as shown in Fig. 1(c). For $u > \varepsilon$ the horn avoided crossing appears [27] [see Fig. 1(d)]. As u increases, more SPs emerge.

Careful inspection shows that the nonlinear breakdown of adiabaticity goes beyond the bifurcation diagram analysis [43]. In Fig. 2(a), inefficient transfer at low $\dot{x}$ is obtained even for $u < \varepsilon$, where no horn crossing is present. Population oscillations, indicating nonadiabaticity, are boosted only during the marked intervals in Fig. 2(a), for which the adiabatic bifurcation diagram exhibits no special nonlinear features. Moreover, as shown in Fig. 2(c), while for $u > \varepsilon$ the horn crossing does appear in an early stage, adiabaticity breaks down even if the system is initiated *after* it. Here, too, the growth of population oscillations does not correlate with the avoided crossing or any other feature in the bifurcation diagram.

Another unique finding is the dependence of transfer efficiency on sweep rate. Oddly, the efficiency increases for

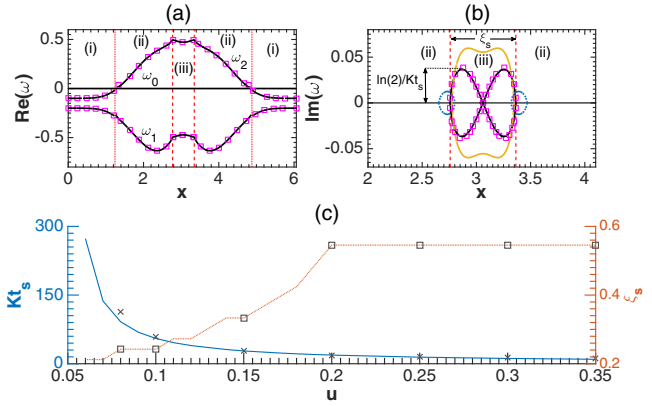

FIG. 3. Stability analysis: (a) $\mathrm{Re}(\omega_j)$ for $u = 0.2$. The followed SP is swapped from an energy maximum in region (i) to a saddle point in regions (ii) and (iii). (b) $\mathrm{Im}(\omega_j)$ for $u = 0.1$ (dotted), 0.2 (solid), 0.3 (dash dotted). It becomes nonzero in region (iii), implying loss of dynamical stability. Square markers in (a),(b) denote approximate analytical solutions [43] for $u = 0.2$. The parameters ξ_s and t_s are extracted as shown. (c) Dependence of ξ_s (dotted) and t_s (solid) on u. Markers denote ξ_s (□) and t_s (×) as obtained from spreading simulations of a semiclassical cloud (see Supplemental Material [43]).

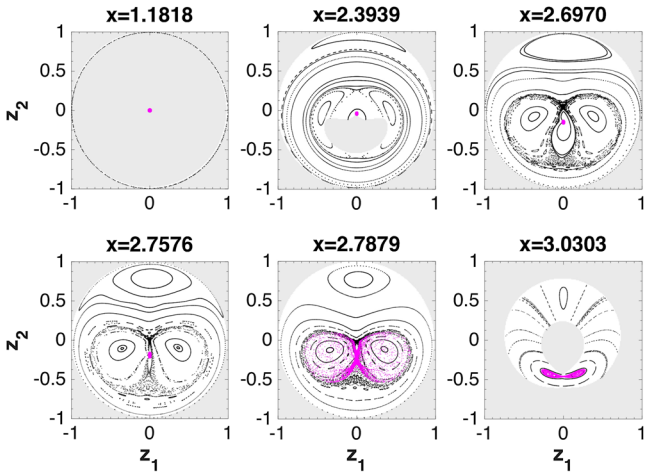

FIG. 4. Poincaré sections for the fixed x Hamiltonian at representative values of x. Here $u = 0.22$. The energy in all panels is $E = E(\mathrm{SP})$ of the followed SP. The cross section is taken through the $n_2 = n_2(\mathrm{SP})$ plane of the 3D energy surface. We use polar coordinates $z_1 = r\sin\varphi$, $z_2 = r\cos\varphi$, where $r = [1 - (n/N)]/2$. Magenta dots correspond to a semiclassical cloud, initially localized around the followed SP. Gray shading marks energetically forbidden regions. Note that these panels depict the adiabatic sequence up to the middle point $x \sim 3$. The Poincaré sections at later times mirror the presented panels and contain a second chaotic interval.

faster sweep rates. In fact, as demonstrated in Fig. 2(b), adiabaticity can be restored by speeding up the sweep process only during the marked intervals mentioned above. This prescription obviously has nothing to do with bifurcations of stationary solutions.

Stability analysis.—The followed SP's stability is determined by solving the Bogoliubov equations [32,33] for its quasiparticle modes $(\mathbf{u}_j, \mathbf{v}_j)$ and frequencies ω_j. Defining $\mathcal{L} = \mathcal{H}_0 + 2u\mathcal{P}(\mathbf{a}_{\mathrm{SP}}) - \mu/K$, and $\mathcal{M} = -u\mathcal{P}(\mathbf{a}_{\mathrm{SP}})$, where $\mathbf{a}_{\mathrm{SP}}$ is the state vector at the stationary point, these equations read

$$\begin{pmatrix} \mathcal{L} & \mathcal{M} \\ -\mathcal{M} & -\mathcal{L} \end{pmatrix} \begin{pmatrix} \mathbf{u}_j \\ \mathbf{v}_j \end{pmatrix} = \omega_j \begin{pmatrix} \mathbf{u}_j \\ \mathbf{v}_j \end{pmatrix}. \tag{3}$$

Energetic stability is determined by the signs of $\mathrm{Re}(\omega_j)$, while dynamical instability is indicated by nonvanishing $\mathrm{Im}(\omega_j)$. An analytical approximation for the Bogoliubov frequencies (see Supplemental Material [43]) is in excellent agreement with direct numerical diagonalization (see Fig. 3). The resulting frequencies include the zero mode $\omega_0 = 0$ due to global gauge symmetry [32,33]. From the remaining frequencies $\omega_{1,2}$ it is clear that, while the horn crossing amounts to a transition from a self-trapped energy maximum ($\omega_{1,2} < 0$) to a saddle point ($\omega_1 < 0$, $\omega_2 > 0$), dynamical instability only appears later, in precise agreement with the "adiabaticity killing grounds" of Fig. 2. The breakdown of STIRAP efficiency is thus not due to energetic instability, but rather due to dynamical instability. From these plots, we find the width of the unstable region ξ_s and the characteristic instability time $t_s = \ln 2/\max(\omega)$ at which the fluctuations are doubled. These parameters agree well with numerical simulations of the spreading of a semiclassical cloud around the SP (see Supplemental Material [43]).

Passage through chaos.—In Fig. 4, we show representative Poincaré sections for several x values during the adiabatic passage. The Bose-Hubbard trimer is a two freedom system (two population imbalances and two relative phases serving as conjugate coordinates); hence its phase space is 4D and the fixed energy surfaces are 3D. For a given N and E our dynamical coordinates are the middle site occupation n_2, the population imbalance $n = n_1 - n_3$, and the relative phase $\varphi = \varphi_1 - \varphi_3$. All the trajectories belong to the pertinent energy surface $E = E(\mathrm{SP})$. A trajectory is sampled each time that it intersects the plane $n_2 = n_2(\mathrm{SP})$. Accordingly, we get a section whose coordinates are $\mathbf{z} = (\varphi, n)$. These are displayed as polar coordinates in Fig. 4. Note that the observed structures do not reflect the topography of the energy landscape, but correspond to various periodic orbits, invariant tori, and chaotic regions on the same energy surface. The plotted sections contain a single SP that supports the followed adiabatic eigenstate, while the other "fixed points" are in fact periodic orbits. In each section, we plot the evolution of a cloud that is launched around the followed SP.

The sequence of Poincaré sections reveals the source of dynamical instability. At early times ($x = 1.1818$) the dynamics is interaction dominated and the evolution is

restricted to self-trapped trajectories. Appropriately for an energy maximum, the followed SP is surrounded by an energetically forbidden region (gray). After the horn crossing, the followed SP is an energy saddle, the forbidden region disappears, and an intermediate nonlinear resonance shows up as a "belt" in the Poincaré section ($x = 2.3939$). At larger x, the belt expands and a chaotic strip is formed along its border ($x = 2.6970$). The enclosed "island," containing the followed SP, shrinks down until the SP hits the chaotic strip ($x = 2.7576$). The dynamical instability intervals correspond to the embedding of the followed SP in the chaotic strip, resulting in the quasistochastic spreading of the initially localized distribution over the chaotic region ($x = 2.7879$). The entire progression takes place on a single 3D energy surface and has no trace in the adiabatic energy diagram.

Adiabaticity threshold.—The draining of the SP region can be avoided if the chaotic interval ξ_s is traversed on a shorter timescale than the instability time t_s. Thus, a low sweep rate adiabaticity threshold should exist. Combining with the standard adiabaticity condition, we deduce that high STIRAP efficiency is maintained for

$$\frac{\xi_s}{t_s} < \dot{x} < \frac{1}{3\pi} K. \tag{4}$$

The upper limit is required for 96% efficiency [2] and ensures small probability for nonadiabatic transitions in the transverse (energy) direction. If $\dot{x}$ is constant throughout the evolution, the adiabaticity threshold condition translates into $\tau < t_s/x_s$ for the sweep time. For larger u, the ξ_s range becomes larger, while t_s becomes smaller [see Fig. 3(c)]. Consequently, the adiabaticity threshold is monotonically increasing as a function of u.

Horn versus belt resonance.—The horn avoided crossing [27] is a 1:1 resonance (frequency of the first site matches the frequency of the second due to interaction). It is born provided $u > \varepsilon$ such that the condition $Un_1 = \mathcal{E}$ can be satisfied. We realize that there is also a nonlinear 2:1 resonance that manifests itself if $u > \varepsilon/2$ (frequency of the first site is half the detuning). It shows up in the Poincaré section as a belt that consist of two islands. This belt is born far away from the followed SP, nevertheless, it can choke the SP in a later stage (Fig. 4).

We note that weak nonadiabatic effects due to horn resonance can be detected as well, but for $u > 0$, as discussed above, they are overwhelmed by the passage-through-chaos mechanism. In contrast, Poincaré sections for $u < 0$ (not presented) show that the SP does not go through the chaotic strip of the nonlinear belt. Consequently, in the latter case, the passage-through-chaos mechanism becomes irrelevant, and the failure of STIRAP is purely due to the horn crossing.

STIRAP efficiency.—In Fig. 5, we plot the STIRAP efficiency as a function of u for several values of $\dot{x}$, as well

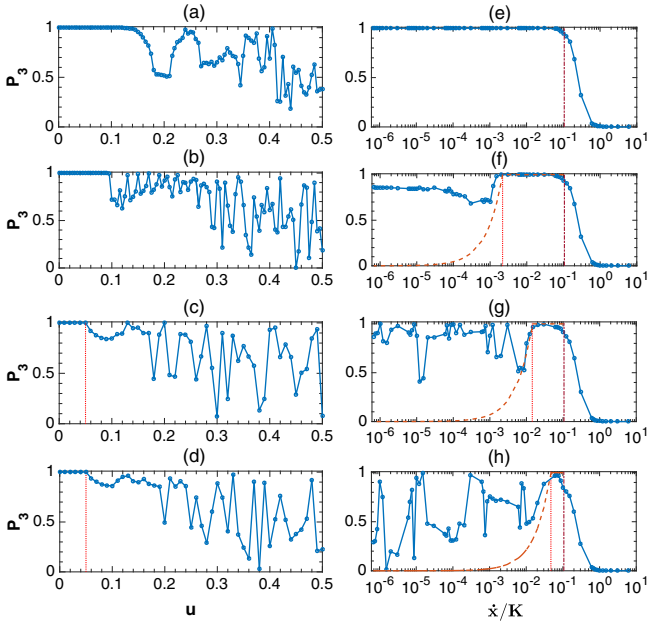

FIG. 5. STIRAP efficiency. P_3 is the population fraction in the target state at the end of the nonlinear STIRAP. (a)–(d) P_3 as a function of u for $\dot{x}/K = 6 \times 10^{-3}, 6 \times 10^{-4}, 6 \times 10^{-6}, 6 \times 10^{-7}$, respectively. Vertical lines in (c),(d) mark the chaoticity threshold $u = \varepsilon/2$. (e)–(h) Present P_3 as a function of the sweep rate $\dot{x}$ for $u = 0.05, 0.1, 0.2, 0.3$, respectively. Vertical lines mark the range of adiabaticity [condition (4)]. The estimated SP survival probability Eq. (5) is plotted as orange dashed line.

as the complimentary dependence on $\dot{x}$ at fixed u. The shrinking of the high efficiency u range as $\dot{x}$ is decreased and reflects the breakdown of adiabaticity due to the passage-through-chaos mechanism. In the adiabatic regime Figs. 5(c) and 5(d), the range of ~100% efficiency is restricted by the "chaoticity threshold" ($|u| < |\varepsilon|/2$) below which no stochastic strips are formed. We note that a similar plot in Ref. [27] corresponds to an intermediate value of $\dot{x}$; hence it does not represent the adiabatic regime.

Looking at the right panels of Fig. 5, we see that below the chaoticity limit [Fig. 5(e)] there is no breakdown in the slow sweep limit, and the efficiency is monotonically decreasing with the rate, just as in the linear case. Once chaos sets in Figs. 5(f)–5(h), high efficiency can still be maintained if condition (4) is satisfied. As u is further increased, the high efficiency range between the slow and fast sweep boundaries shrinks, until the two inequalities of Eq. (4) cannot be satisfied simultaneously Fig. 5(h).

The transfer probability P_3 can be written as a sum $P_{\text{surv}} + P_{\text{scat}}$, where P_{surv} is the probability for survival in the SP region, while P_{scat} the scattered component. The former can be estimated as follows: The spreading trajectories in the stochastic region have frequencies $\omega \in [0, 1/t_s]$ with roughly uniform distribution. Trajectories that survive in the SP region satisfy $\omega \times (\xi_s/\dot{x}) < 1$; hence their fraction is

$$P_{\rm surv} = \min\{(t_s/\xi_s)\dot{x}, 1\}. \quad (5)$$

This estimate can serve as a lower bound for the STIRAP efficiency as illustrated in Figs. 5(f)–5(h).

Conclusions.—The physics of three-mode adiabatic passage schemes is more intricate than that of the nonlinear Landau-Zener paradigm. The latter relies entirely on energetic stability, which is endangered by bifurcations of the followed SP. By contrast, the failure of adiabatic passage in nonintegrable systems is related to dynamical instability on a single multidimensional energy surface, containing both quasi-integrable and chaotic regions. Consequently, adiabatic passage efficiency can be improved by faster variation of the control parameters. The role of chaos as an optional tool to control the outcome of a STIRAP scheme has been pointed in [44,45] in a different context: there the chaos was due to the laser frequencies, and the analysis was based on Floquet theory that goes beyond the traditional rotating-wave approximation of Eq. (1).

This research was supported by the Israel Science Foundation (Grant No. 283/18).

[1] U. Gaubatz, P. Rudecki, S. Schiemann, and K. Bergmann, J. Chem. Phys. **92**, 5363 (1990).
[2] N. V. Vitanov, A. A. Rangelov, B. W. Shore, and K. Bergmann, Rev. Mod. Phys. **89**, 015006 (2017).
[3] J. W. Fleischer, G. Bartal, O. Cohen, T. Schwartz, O. Manela, B. Freedman, M. Segev, H. Buljan, and N. K. Efremidis, Opt. Express **13**, 1780 (2005).
[4] Y. Lahini, F. Pozzi, M. Sorel, R. Morandotti, D. N. Christodoulides, and Y. Silberberg, Phys. Rev. Lett. **101**, 193901 (2008).
[5] O. Zobay and B. M. Garraway, Phys. Rev. A **61**, 033603 (2000).
[6] B. Wu and Q. Niu, Phys. Rev. A **61**, 023402 (2000).
[7] J. Liu, L. Fu, B.-Y. Ou, S.-G. Chen, D.-I. Choi, B. Wu, and Q. Niu, Phys. Rev. A **66**, 023404 (2002).
[8] J. Liu, B. Wu, and Q. Niu, Phys. Rev. Lett. **90**, 170404 (2003).
[9] D. Witthaut, E. M. Graefe, and H. J. Korsch, Phys. Rev. A **73**, 063609 (2006).
[10] D. Witthaut, F. Trimborn, V. Kegel, and H. J. Korsch, Phys. Rev. A **83**, 013609 (2011).
[11] A. M. Ishkhanyan, Europhys. Lett. **90**, 30007 (2010).
[12] J. R. Anglin, Phys. Rev. A **67**, 051601(R) (2003).
[13] A. Altland and V. Gurarie, Phys. Rev. Lett. **100**, 063602 (2008).
[14] F. Trimborn, D. Witthaut, V. Kegel, and H. J. Korsch, New J. Phys. **12**, 053010 (2010).
[15] K. Smith-Mannschott, M. Chuchem, M. Hiller, T. Kottos, and D. Cohen, Phys. Rev. Lett. **102**, 230401 (2009).
[16] Y.-A. Chen, S. D. Huber, S. Trotzky, I. Bloch, and E. Altman, Nat. Phys. **7**, 61 (2011).
[17] S. F. Caballero-Benitez and R. Paredes, Phys. Rev. A **85**, 023605 (2012).
[18] J. Javanainen and M. Mackie, Phys. Rev. A **59**, R3186(R) (1999).
[19] V. A. Yurovsky, A. Ben-Reuven, P. S. Julienne, and C. J. Williams, Phys. Rev. A **62**, 043605 (2000).
[20] D. J. Heinzen, R. Wynar, P. D. Drummond, and K. V. Kheruntsyan, Phys. Rev. Lett. **84**, 5029 (2000).
[21] A. Ishkhanyan, M. Mackie, A. Carmichael, P. L. Gould, and J. Javanainen, Phys. Rev. A **69**, 043612 (2004).
[22] E. Altman and A. Vishwanath, Phys. Rev. Lett. **95**, 110404 (2005).
[23] E. Pazy, I. Tikhonenkov, Y. B. Band, M. Fleischhauer, and A. Vardi, Phys. Rev. Lett. **95**, 170403 (2005).
[24] I. Tikhonenkov, E. Pazy, Y. B. Band, M. Fleischhauer, and A. Vardi, Phys. Rev. A **73**, 043605 (2006).
[25] J. Liu, B. Liu, and L. B. Fu, Phys. Rev. A **78**, 013618 (2008).
[26] J. Liu, L.-B. Fu, B. Liu, and B. Wu, New J. Phys. **10**, 123018 (2008).
[27] E. M. Graefe, H. J. Korsch, and D. Witthaut, Phys. Rev. A **73**, 013617 (2006).
[28] M. Rab, J. H. Cole, N. G. Parker, A. D. Greentree, L. C. L. Hollenberg, and A. M. Martin, Phys. Rev. A **77**, 061602(R) (2008).
[29] C. J. Bradly, M. Rab, A. D. Greentree, and A. M. Martin, Phys. Rev. A **85**, 053609 (2012).
[30] J. Polo, A. Benseny, Th. Busch, V. Ahufinger, and J. Mompart, New J. Phys. **18**, 015010 (2016).
[31] M. Dupont-Nivet, M. Casiulis, T. Laudat, C. I. Westbrook, and S. Schwartz, Phys. Rev. A **91**, 053420 (2015).
[32] N. N. Bogoliubov, Il Nuovo Cimento **7**, 794 (1958).
[33] C. Pethick and H. Smith, *Bose-Einstein Condensation in Dilute Gases* (Cambridge University Press, Cambridge, England, 2002), Chap. 7, p. 174.
[34] G. Arwas, A. Vardi, and D. Cohen, Sci. Rep. **5**, 13433 (2015).
[35] J. C. Eilbeck, G. P. Tsironis, and S. K. Turitsyn, Phys. Scr. **52**, 386 (1995).
[36] D. Hennig, H. Gabriel, M. F. Jorgensen, P. L. Christiansen, and C. B. Clausen, Phys. Rev. E **51**, 2870 (1995).
[37] R. Franzosi and V. Penna, Phys. Rev. E **67**, 046227 (2003).
[38] S. Flach and V. Fleurov, J. Phys. Condens. Matter **9**, 7039 (1997).
[39] K. Nemoto, C. A. Holmes, G. J. Milburn, and W. J. Munro, Phys. Rev. A **63**, 013604 (2000).
[40] R. Franzosi and V. Penna, Phys. Rev. A **65**, 013601 (2001).
[41] M. Hiller, T. Kottos, and T. Geisel, Phys. Rev. A **73**, 061604 (R) (2006).
[42] I. Tikhonenkov, A. Vardi, J. R. Anglin, and D. Cohen, Phys. Rev. Lett. **110**, 050401 (2013).
[43] See Supplemental Material at http://link.aps.org/supplemental/10.1103/PhysRevLett.121.250405 for further discussion of the role played by the horn crossing as opposed to chaos; the details of the Poincare sections; the calculation of the Bogoliubov frequencies; and the spreading simulations.
[44] K. Na and L. E. Reichl, Phys. Rev. A **70**, 063405 (2004).
[45] K. Na and L. E. Reichl, Phys. Rev. A **72**, 013402 (2005).